

## Article

# Zircon U-Pb Dating of the Irizar Granite in the Central Victoria Land, Antarctica: Insights into the Tectonic Evolution along the Ross Orogen

Shaocong Chen <sup>1</sup>, Yingchun Cui <sup>1,\*</sup>, Shi Zong <sup>1</sup>, Hao Zhang <sup>1</sup>, Weixuan Wang <sup>1</sup>, Shenggui Li <sup>1</sup> and Chenguang Liu <sup>2</sup> 

<sup>1</sup> MNR Key Laboratory for Polar Science, Polar Research Institute of China, Ministry of Natural Resources, Shanghai 200136, China; chenshaocong@pric.org.cn (S.C.); zongshi@pric.org.cn (S.Z.); zhanghao@pric.org.cn (H.Z.); wangweixuan@pric.org.cn (W.W.); lishenggui@pric.org.cn (S.L.)

<sup>2</sup> Key Laboratory of Marine Geology and Metallogeny, First Institute of Oceanography, Ministry of Natural Resources, Qingdao 266061, China; lcg@fio.org.cn

\* Correspondence: cuiyingchun@pric.org.cn

**Abstract:** It has been accepted that granitoids of the Irizar unit in the Central Victoria Land (Antarctica), as an important part of the Granite Harbour Intrusives, were formed in a post-collisional setting during the Ross orogeny along the margin of east Gondwana. However, the emplacement ages of the Irizar unit remain poorly constrained, making it difficult to form a more complete picture of the geodynamic evolution of the Ross orogen and its counterpart (Delamerian orogen) in southeast Australia. In this work, four syenogranite samples from the Irizar unit were chosen for SHRIMP zircon U-Pb dating, which yielded ages of 507.8–489.7 Ma. The new geochronological data indicate that the post-collisional extension in the Central Victoria Land had begun by ~508 Ma, much earlier than previously thought (i.e., 490–480 Ma). Integrated with U-Pb ages for Early Paleozoic granitoids from the literature, the Ross–Delamerian orogen shows that the post-collisional granitic magmatism initiated at ~515 Ma in the Central Transantarctic Mountains and northward systematically decreased to ~508 Ma in the Victoria Land, and then to ~487 Ma in southeast Australia. This can be explained well by the propagating northward transition from pre- and syn-collisional compression to post-collisional extension.

**Keywords:** SHRIMP zircon U-Pb age; tectonic setting of the Irizar granite; Central Victoria Land; Antarctica; Ross–Delamerian orogen



**Citation:** Chen, S.; Cui, Y.; Zong, S.; Zhang, H.; Wang, W.; Li, S.; Liu, C. Zircon U-Pb Dating of the Irizar Granite in the Central Victoria Land, Antarctica: Insights into the Tectonic Evolution along the Ross Orogen. *Minerals* **2024**, *14*, 301.

<https://doi.org/10.3390/min14030301>

Academic Editor: Manuel Francisco Pereira

Received: 4 February 2024

Revised: 8 March 2024

Accepted: 9 March 2024

Published: 13 March 2024



**Copyright:** © 2024 by the authors. Licensee MDPI, Basel, Switzerland. This article is an open access article distributed under the terms and conditions of the Creative Commons Attribution (CC BY) license (<https://creativecommons.org/licenses/by/4.0/>).

## 1. Introduction

During the Latest Neoproterozoic to Early Paleozoic time, the paleo-Pacific margin of the Gondwana supercontinent turned from passive margin sedimentation to convergent margin activity [1,2]. This convergent orogeny resulted in the formation of a large accretionary orogen, in response to the subduction of the paleo-Pacific oceanic lithosphere beneath the margin of east Gondwana and subsequent arc–continent collision [3–6]. This orogen is known regionally as Ross in Antarctica and as Delamerian in southeastern Australia [3,7–11] (Figure 1A). Due to the geographic remoteness and generous cover of ice and snow, the tectonic evolution along the Ross orogen remains enigmatic, compared to orogens in other continents.

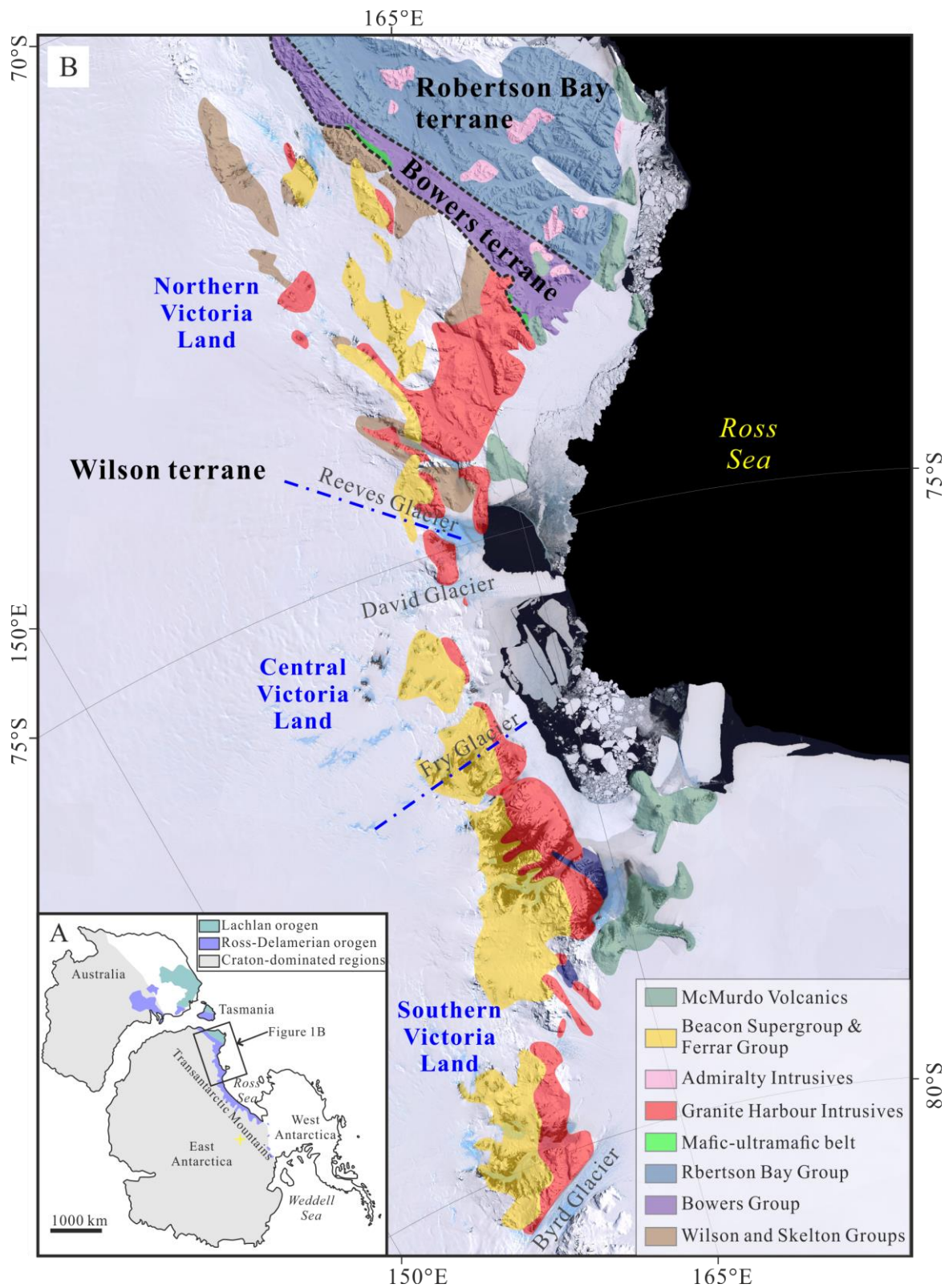


**Figure 1.** (A) Pre-Gondwana-breakup configuration of Antarctica and Australia, showing Paleozoic Ross–Delamerian orogen [11]. (B) Sketch geological map of Victoria Land (Antarctica), showing the distribution of the Granite Harbour Intrusives (modified from [12]). Satellite image of the Victoria Land is obtained from the Landsat Image Mosaic of Antarctica (LIMA) Project accessed on 11 July 2023 (<http://lima.usgs.gov>).

One of the hallmarks of the Ross orogen is the widespread emplacement of granitoids, which, together with minor mafic-ultramafic rocks, are collectively referred to as the Granite Harbour Intrusives (GHI) [12,13] (Figure 1B). Previous studies have shown that they were formed through all stages of the Ross orogenic development from pre- and syn- to post-kinematic settings [14–18]. Available geochronological data for the GHI magmatism, as well as the metamorphism, deformation, and sedimentation in this orogen, have indicated an overall northward younging trend of the initiation of subduction from the Central Transantarctic Mountains at ~580–540 Ma toward Victoria Land at ~550–530 Ma and to southeastern Australia at ~515 Ma, which supports oblique convergence along the Gondwana margin [9,14,18–22]. By contrast, Foden et al. [9] and Rocchi et al. [11,23] proposed that the post-collisional extension occurred synchronously on both the Ross and Delamerian sides at ~490–480 Ma, according to a comparison of radiometric ages for the bimodal, post-collisional igneous rocks on both sides. However, many of these ages are less reliable whole-rock Rb-Sr and mica/amphibole Ar-Ar isochrons [24–26]. Available U/Pb upper intercept ages of ~490–488 Ma for the post-collisional Irizar granites in the Central Victoria Land [11] should also be treated with caution. This is because the interpretation of the zircon ages has not been verified by cathodoluminescence (CL) studies and zircons from granitoids in the Victoria Land usually display complex internal textures [14,18,27,28]. Consequently, questions remain concerning the timing of the transition pre- and syn-collisional compression to post-collisional extension, especially in the Central Victoria Land section, making it difficult to form a more complete picture of the geodynamic evolution along the Ross (–Delamerian) orogen.

In this contribution, we report new zircon U-Pb ages for the undeformed Irizar granite in the Central Victoria Land (Antarctica), which displays geochemical features typical of post-collisional granitoids [11]. The new data allow us not only to provide better age controls on the emplacement of the Irizar granites, but also to elucidate the tectono-magmatic evolution of the Ross–Delamerian orogen.

## 2. Geological Setting

The 3500 km long Transantarctic Mountains, a major tectonic domain in Antarctica, run across entire Antarctica from the Northern Victoria Land to the Pensacola Mountains and separate cratonic East Antarctica from tectonically active West Antarctica [29] (Figure 1A). Bordering the northeast side of the Transantarctic Mountains is the late Neoproterozoic to Cambrian Ross orogen, [7,12,30] (Figure 1A), which belongs to the greater Terra Australis orogen developed along the entire eastern margin of the Gondwana supercontinent from Neoproterozoic to late Paleozoic [3].

The Victoria Land occupies a critical position at the former juncture between southeast Australia and the Transantarctic Mountains [3,8,30–32] (Figure 1). It is composed of three fault-bounded litho-tectonic units: the Wilson, Bowers, and Robertson Bay terranes, from west to east [33,34] (Figure 1B). The Wilson terrane is interpreted as an active continental margin of the East Antarctic craton during the Ross period [23,35]. It mainly comprises metasedimentary, like schists, gneisses, migmatites and minor marbles of the Wilson group in the northern section and the Skelton group in the southern section [12,36,37]. The protolith of these metamorphic rocks represents the Neoproterozoic rift-margin deposits with a combined cratonic and early Ross Orogen provenance [38–41]. They were deformed into overturned folds and thrusts in the latest Precambrian to early Paleozoic. After the Ross orogeny, they were unconformably overlain by Late Paleozoic and Early Mesozoic sedimentary and volcanic successions of the Beacon supergroup and Ferrar group (Figure 1B). Both the Bowers and Robertson Bay terranes comprise weakly-metamorphosed turbiditic greywacke, sandstone, argillite, shale, and locally minor conglomerate [42,43]. Detrital white micas and zircons yielded depositional ages of ~550–480 Ma and a predominant sediment provenance from the emerging Ross orogen [39,40]. They are interpreted as a Late Cambrian or Ordovician turbiditic sequence deposited in an accretionary setting [40]. These rocks were characteristically deformed into upright folds. It is noteworthy that

the two terranes were separated by faults, but their relationships remain poorly constrained. At the boundary between the Wilson and Bowers terranes, a discontinuous metavolcanic belt occurs of amphibolite- to eclogite-facies mafic-ultramafic rocks with ages of ~530–500 Ma [6,44] (Figure 1B). They have arc tholeiitic, calc-alkaline and alkaline geochemical affinities, and are traditionally interpreted as part of an intra-oceanic island arc [6,34,45,46]. McMurdo volcanics and glacial deposits are common in the eastern margins of the Wilson, Bowers, and Robertson Bay terranes, and define the Cenozoic phase of the geological evolution in the Victoria Land.

Granitic rocks are widespread in the Victoria Land and can be divided into two major groups: the GHI confined to the Wilson terrane and the Admiralty Intrusives in the Bowers and Robertson Bay terranes [31]. The former comprises a variety of lithologies from hornblende-biotite tonalite and granodiorite to granite, leucogranite, and syenite. They show meta-luminous I-type to peraluminous S-type and high-K calc-alkaline to shoshonitic affinities [17,18,31,47–49]. Zircon U-Pb dating shows that they were emplaced over a long period from ~580 Ma to 470 Ma, with the main magmatic pulse between ~530 Ma and 480 Ma [11,12,18,27,28,50–54]. Petrographic, mineralogical and geochemical data have demonstrated that they originated from melting of heterogeneous crustal sources with varying mixtures of mantle-derived components [14–18]. In contrast, the Admiralty Intrusives refers to a granitic suite, mainly of granodiorite, tonalite, diorite, monzogranite, and related aplitic dikes and pegmatite with calc-alkaline to calcic and I-type affinities [12,31,47]. At present, there are no published zircon U-Pb age constraints on the Admiralty Intrusives, and less reliable K-Ar and Rb-Sr whole rock-mineral isochron ages indicated that they were emplaced at ~390–280 Ma [55,56]. The age and the chemical composition of Admiralty's plutonic rocks are different from those of the GHI.

The Central Victoria Land, bounded by the Reeves and Fry Glaciers, is located within the Wilson terrane [57] (Figures 1B and 2). Based on field relationships, and the petrological, mineralogical and geochemical compositions, the GHI rocks in this area can be subdivided into three main units: the Larsen granodiorite, Irizar granite, and Vegetation lamprophyre [11,58,59] (Figure 2). The Larsen granodiorite is distributed along the entire coast of the Central Victoria Land (Figure 2) and extends southwards to the South Victoria Land [58]. This unit has a wide compositional range spanning from quartz diorite and tonalite, through granodiorite, to adamellite and monzonitic granite. The strong deformation evidenced by the development of augen gneiss, with a strong foliation, suggests the pre- to syn-tectonic nature of the Larsen granodiorite [58]. To date, reliable radiometric dates are still lacking for the Larsen granodiorite. The Irizar granite occurs as stock-like syenogranite bodies throughout the Central Victoria Land (Figure 2). It intruded into the Larsen granodiorite with steep and sharp contacts and chilled margins [58]. The Irizar granite is characteristically undeformed and much more homogeneous in composition, compared to the Larsen unit. The Vegetation lamprophyre crops out dominantly in the northern section (Figure 2), as NE–NNE-trending subvertical dike swarms, with widths of an individual dike ranging from a few centimeters to over 30 m. Skinner and Ricker [58] noted that the Vegetation lamprophyre dikes crosscut both the Larsen and Irizar units (Figure 2), but zircon U-Pb, whole-rock Rb-Sr, and biotite/amphibole Ar-Ar dating yielded indistinguishable ages of ~490 Ma for the two units [11,26,60]. Based on the similar geochemical features and Sr-Nd isotope compositions, Rocchi et al. [11] proposed that the two units were genetically related, with the Irizar granite resulting from high-degree partial melting of underplated, mantle-derived materials similar in composition to the Vegetation lamprophyre.

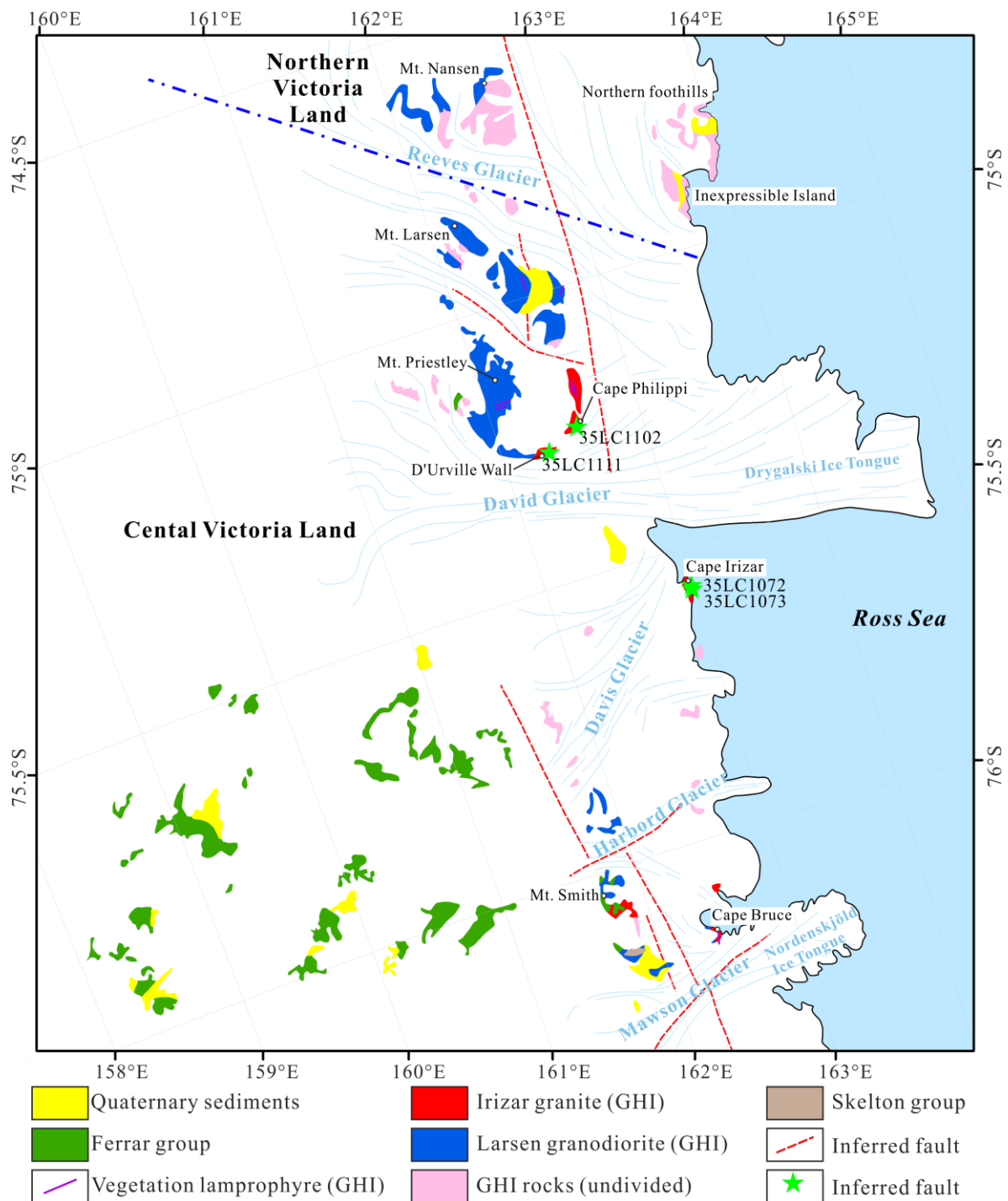


**Figure 2.** Sketch map of the Central Victoria Land, showing the distribution of Larsen granodiorite and Irizar granite (modified from [57]). Abbreviations: GHI, Granite Harbour Intrusives; Mt., Mount.

### 3. Petrology of the Irizar Granite

The Irizar unit consists of pinkish, medium- to coarse-grained syenogranite, and mainly comprises K-feldspar (43–50 vol.%), plagioclase (20–25 vol.%), quartz (20–25 vol.%), biotite (2–5 vol.%) and, locally, amphibole (1–3 vol.%), with accessory zircon, allanite, and Fe-Ti oxides (Figure 3). K-feldspar is mainly subhedral to anhedral orthoclase and perthite, forming large crystals with diameters of up to 7 mm (Figure 3A,D,E). It is often intergrown with quartz and plagioclase (Figure 3A,D), and occasionally includes fine-grained euhedral to subhedral plagioclase (Figure 3E). Plagioclase crystals with diameters of up to 5 mm

are euhedral to subhedral with obvious polysynthetic twinning (Figure 3A,D). Locally, sericitized cores can be observed in plagioclase (Figure 3B). Quartz is mostly present as subhedral to anhedral grains (Figure 3). Biotite is mainly present as subhedral fine-grained flakes, occurring interstitially between K-feldspar, plagioclase, and quartz (Figure 3B,D). Locally, biotite is altered to chlorite. Amphibole is also observed in some samples, and it occurs as subhedral crystals with diameters up to 2 mm and diagnostic cleavages at  $\sim 120^\circ$  (Figure 3F). Locally, amphibole encloses fine-grained biotite flakes. The accessory allanite and Fe-Ti oxides are typically intergrown with or enclosed by the mafic minerals. Previous whole-rock elemental compositions of the Irizar granite [11] are plotted in the granite and syenogranite fields in the TAS ( $\text{SiO}_2$  vs.  $\text{Na}_2\text{O} + \text{K}_2\text{O}$ ; [61]; Figure 4A) and Q–A–P ([62]; Figure 4B) diagrams, respectively, consistent with the petrographic observation. The biotite and amphibole compositions also indicate an alkaline affinity for the Irizar granite [11].

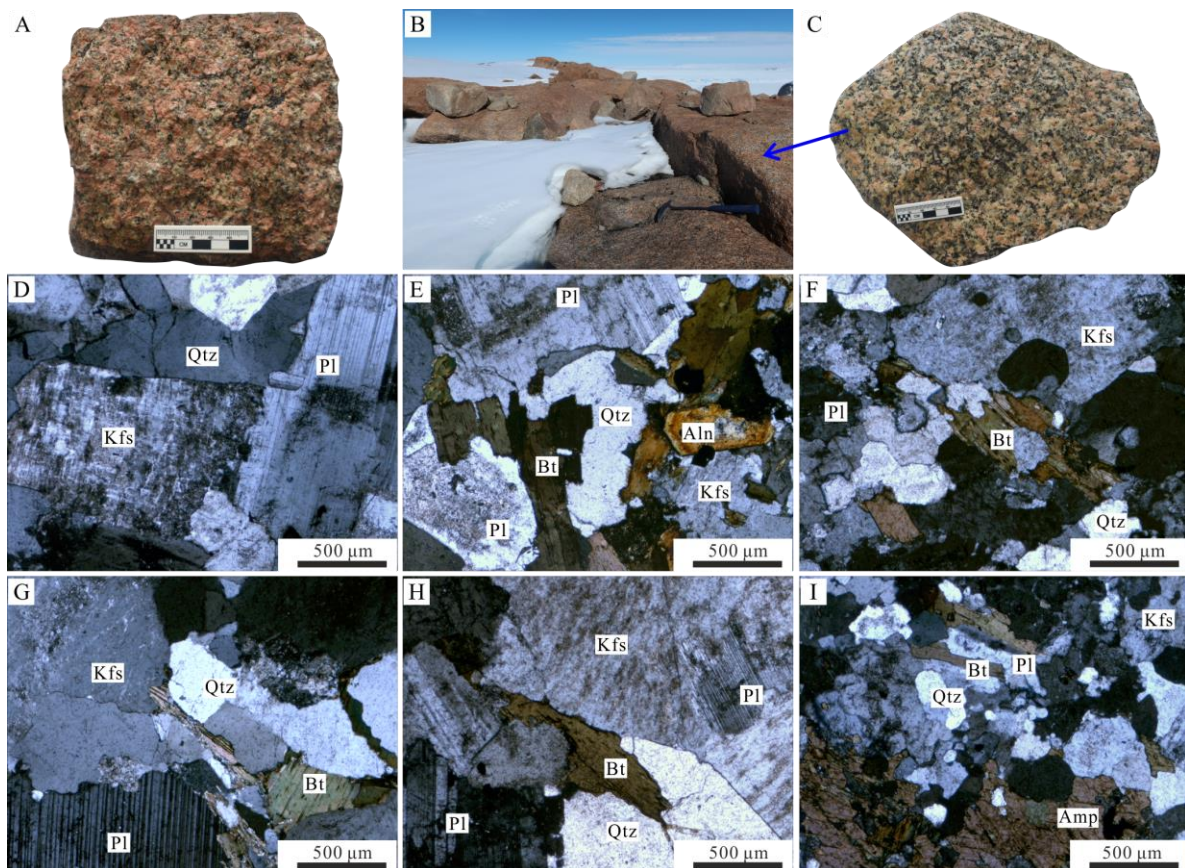


**Figure 3.** Representative microphotographs of the Irizar granite. (A) Syenogranite of the Irizar unit at Cape Irizar; (B,C) syenogranite of the Irizar unit at D'Urville; (D) the Irizar granite consists of coarse-grained quartz, plagioclase, and K-feldspar (cross-polarized light); (E) allanite occurs locally in the Irizar granite (cross-polarized light); (F,G) the Irizar granite consists of coarse-grained quartz, plagioclase, K-feldspar, and biotite (cross-polarized light); (H) plagioclase is enclosed by K-feldspar (cross-polarized light); (I) amphibole occurs locally in the Irizar granite (cross-polarized light). Abbreviations: Amp, Amphibole; Qtz, quartz; Pl, plagioclase; Kfs, K-feldspar; Bt, biotite; Ttn, titanite; Aln, allanite.

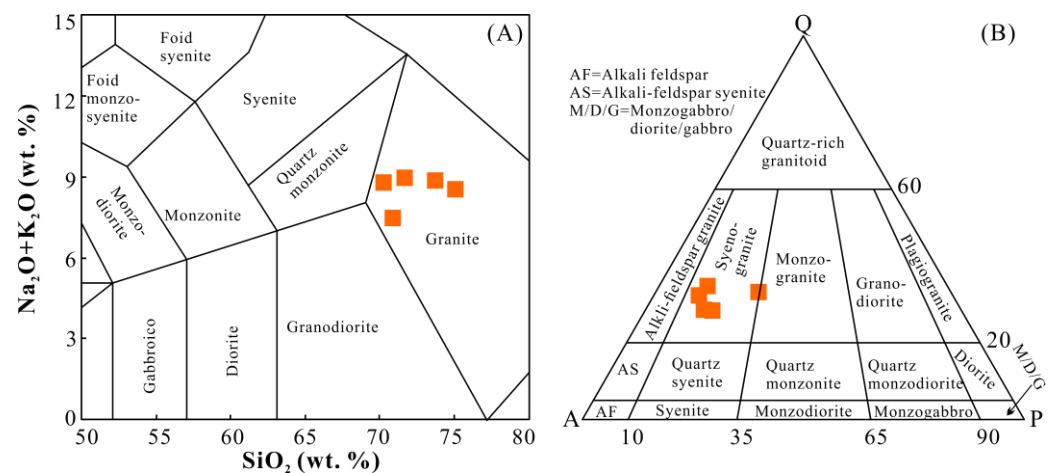


**Figure 4.** (A)  $\text{SiO}_2\text{--Na}_2\text{O} + \text{K}_2\text{O}$  [61], (B) Q–A–P modal classification [62]. Elemental composition for the Irizar granite is collected from [11]. Compositions of the Irizar syenogranite are shown as orange squares.

#### 4. Analytical Methods

Four syenogranite samples of the Irizar granite from the Central Victoria Land (samples 35LC107-2 and 35LC107-3 from the Cape Irizar, sample 35LC110-2 from the Cape Philippi, and sample 35LC111-1 from the D’Urville Wall; Figure 2), were selected for SHRIMP zircon U–Pb dating. Zircons in the samples were separated using conventional density and magnetic separation techniques, and then handpicked under a binocular microscope. The zircon grains were mounted in epoxy for polishing. Cathodoluminescence (CL) images were acquired at the Beijing SHRIMP Center, Chinese Academy of Geological Sciences, Beijing, China, to examine their internal structure prior to the U–Pb dating. Zircon U–Pb dating was carried out using SHRIMP II at the Beijing SHRIMP Center (Beijing, China). The SHRIMP II analytical procedure was similar to that described by Williams [63]. A primary  $25\ \mu\text{m}\ \text{O}^{2-}$  ion beam of 3–6 nA was used to bombard the surfaces of the zircons. Prior to each analysis, the surface common Pb was reduced or eliminated by rastering of the primary beam for 120–200 s, with five scans for each analysis. Standard zircons for elemental abundance calibration included 91,500 ( $U = 91\ \text{ppm}$ ), SL13 ( $U = 238\ \text{ppm}$ ), and M257 ( $U = 840\ \text{ppm}$ ) [63–65]. TEMORA with a  $^{206}\text{Pb}/^{238}\text{U}$  age of 417 Ma was used for calibration [66] and was analyzed after every three sample analyses. Data processing was carried out with the Squid and Isoplot programs [67]. Common Pb corrections were based on the measured  $^{204}\text{Pb}$  contents. Uncertainties for individual analyses are quoted at  $1\sigma$ , and errors for weighted mean ages are quoted at the 95% confidence level.

#### 5. Results

The analytical results of the zircon U–Pb dating are listed in Supplementary Table S1.

The analyzed zircon grains are typically colorless to light yellow and transparent. Apart from the influence of comminution, the zircon grains occur as subhedral to euhedral prismatic crystals, with lengths varying from 30 to  $180\ \mu\text{m}$  and length/width ratio in the range of 1:1 to 3:1 (Figure 5). As shown in the representative CL images (Figure 5), most of the zircons have concentric oscillatory zoning, indicating a magmatic origin [68]. Some zircon grains show chaotic textures and poorly-developed oscillatory zoning, and they often contain dark zones or bands (Figure 5A—35LC107-2@13 and C-35LC110-2@17), indicative of high U concentrations and consequent metamictization by radioactive damage [69]. A few zircons have inherited cores, which are generally smaller than the spot size ( $<25\ \mu\text{m}$ ) of the SHRIMP zircon U–Pb dating technique (Figure 5C—35LC110-2@12). Zircons analyzed from the four samples have Th/U ratios ranging from 0.09 to 1.27 with average values 0.48–0.59 (Table S1), consistent with a magmatic origin for these zircons [68].

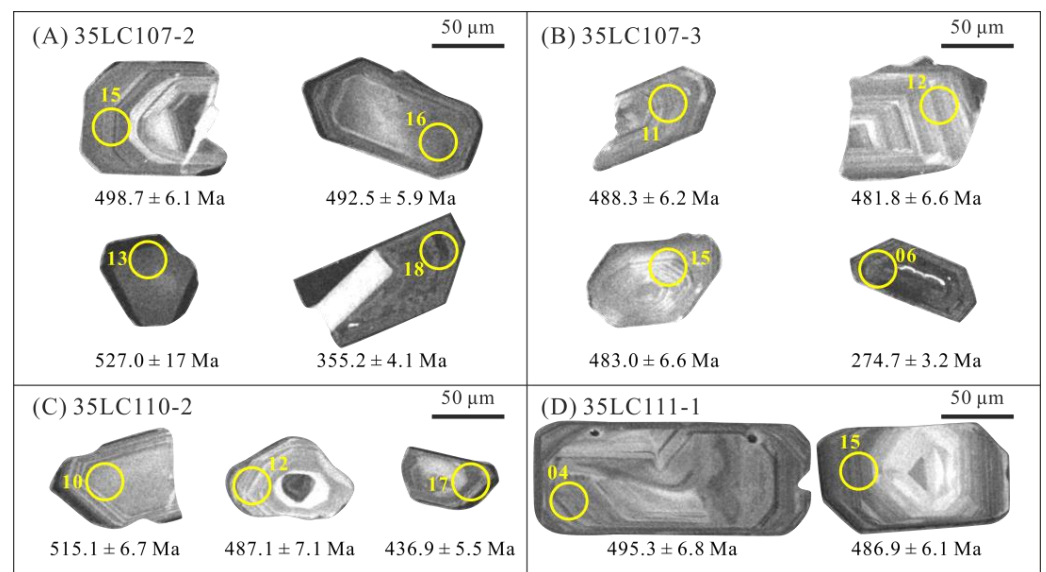


**Figure 5.** Representative cathodoluminescence (CL) images of zircon grains from the Irizar granite in the Central Victoria Land. (A) Sample 35LC107-2; (B) sample 35LC107-3; (C) sample 35LC110-2; (D) sample 35LC111-1. The yellow circles indicate zircon in situ U-Pb isotope analyses. Apparent ages are also shown.

Eighteen zircon spots were analyzed for sample 35LC107-2. Most analyses are slightly discordant, with  $^{207}\text{Pb}/^{206}\text{Pb}$  apparent ages ranging from ~527 Ma to 355 Ma (Table S1). Among them, the 15 least discordant spots fall on or near the concordia curve and have  $^{206}\text{Pb}/^{238}\text{U}$  apparent ages varying from ~485 Ma to 506 Ma (Table S1), yielding a weighted mean age of  $498.3 \pm 3.2$  Ma (MSWD = 0.8; Figure 6A). In addition, one data point from zircon with a CL-dark band has high U concentration of 1275 ppm and yields an older  $^{206}\text{Pb}/^{238}\text{U}$  apparent age of ~527 Ma (Figure 5C—35LC107-2@13; Table S1). This is probably related to the high-U matrix effect in zircon [70]. Another two data points from structure-damaged zircon have much younger  $^{206}\text{Pb}/^{238}\text{U}$  apparent ages of ~462–355 Ma (Figure 5C—35LC107-2@18; Table S1), probably due to the metamictization of zircons. The three abnormal data points are, thus, not used in the age calculations.

Sixteen zircon spots were analyzed for sample 35LC107-3. Among them, 11 spots with  $^{206}\text{Pb}/^{238}\text{U}$  apparent ages of ~479–497 Ma fall on or near the concordia curve, yielding a concordia age of  $488.9 \pm 1.9$  Ma (MSWD = 22) and a consistent weighted mean age of  $489.7 \pm 3.3$  Ma (MSWD = 1.1; Figure 6B). Another four data points from zircon with chaotic textures have much younger  $^{206}\text{Pb}/^{238}\text{U}$  apparent ages of ~426–235 Ma (Table S1), which are excluded in the age calculations due to apparent Pb-loss.

Seventeen zircon spots were analyzed for sample 35LC110-2. The 15 least discordant data points fall on or near the concordia curve, and the  $^{206}\text{Pb}/^{238}\text{U}$  apparent ages vary from ~487 Ma to 520 Ma (Table S1), yielding a weighted mean age of  $\sim 508 \pm 5$  Ma (MSWD = 1.7; Figure 6C). Two data points from zircon with chaotic textures have younger  $^{206}\text{Pb}/^{238}\text{U}$  apparent ages of ~437–379 Ma (Table S1), which are not included in the age calculations.

Fifteen zircon spots were analyzed for sample 35LC111-1. Their  $^{206}\text{Pb}/^{238}\text{U}$  apparent ages vary from ~484 Ma to 507 Ma (Table S1), and fall on or near the concordia curve, yielding a concordia age of  $496.5 \pm 1.7$  Ma (MSWD = 22) and a consistent weighted mean age of  $498.0 \pm 4.2$  Ma (MSWD = 1.6; Figure 6D).

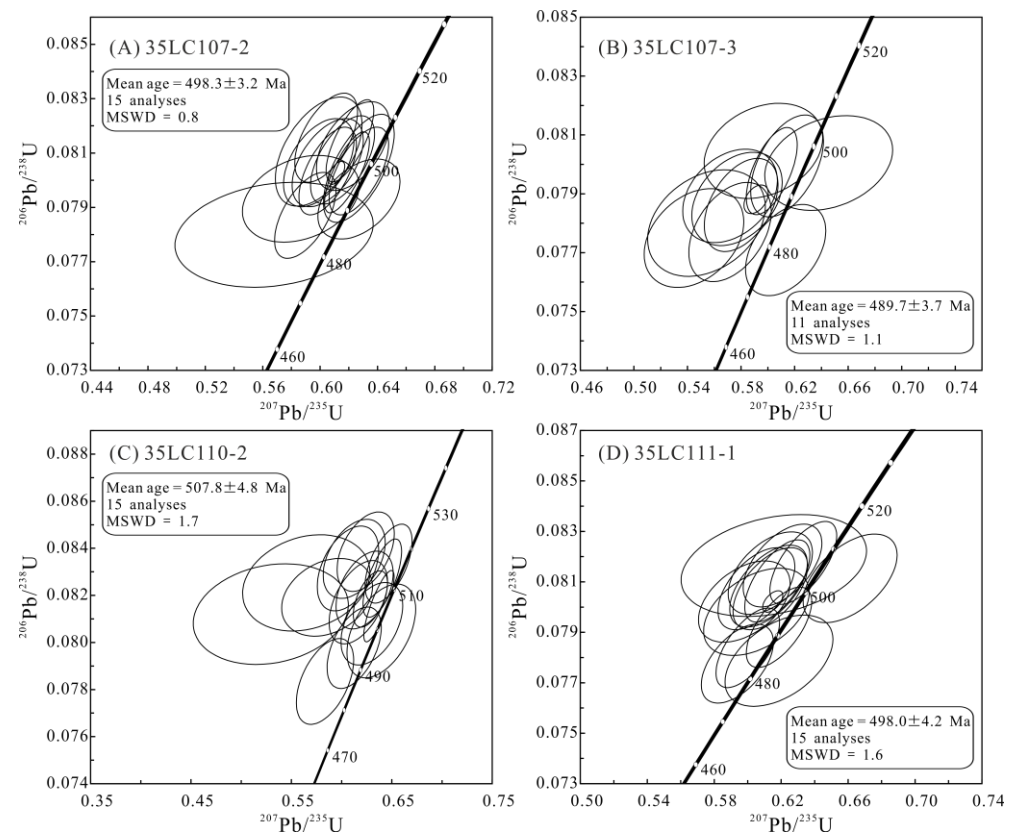


**Figure 6.** SHRIMP zircon U-Pb isotopic concordia diagrams for the Irizar granite in the Central Victoria Land. (A) Sample 35LC107-2; (B) sample 35LC107-3; (C) sample 35LC110-2; (D) sample 35LC111-1.

## 6. Discussion

### 6.1. Timing of the Post-Collisional Magmatism

Until now, geochronological data for the Irizar granite have been limited, although numerous individualized granite plutons, as an important part of the GHI, have been outlined in this area. Di Vincenzo et al. [26] dated biotite and amphibole within the Irizar granite from the Cape Irizar area using Ar-Ar spectrometry and reported cooling ages of ~485–481 Ma. Later, Rocchi et al. [11] reported a whole-rock Rb-Sr isochron age of  $486.1 \pm 8.4$  Ma and two zircon U-Pb upper intercept ages of  $489.9 \pm 4.4$  Ma and  $488.1 \pm 8.7$  Ma for the Irizar granite from the same area. It is noteworthy that the zircon U-Pb upper intercept age was defined by only three analyses of separated zircon grains [11]. Considering the low closure temperatures and susceptibilities to later hydrothermal disturbances of K-Ar and Rb-Sr radiometric systems [71–73], the coincidence of the Ar-Ar and Rb-Sr ages with the zircon U-Pb upper intercept age may indicate that these ages are minimum estimates for the granitic magmatism in the Central Victoria Land. In this study, we obtained two zircon U-Pb ages of ~498–490 Ma for the Irizar granite from the Cape Irizar area (Figure 6A,B), which are broadly in agreement with the previous results. However, the other two samples of the Irizar granite from the Cape Philippi and D’Urville Wall areas provide U-Pb ages of ~508–498 Ma (Figure 6C,D), much older than the emplacement ages for samples from Cape Irizar. Thus, we infer that the Irizar granitic magmatism initiated as early as ~508 Ma and lasted over ~20 Ma to 488 Ma.

The tectonic evolution of orogenic belts is recorded by changes in the associated magmatic composition [74]. The transition from calc-alkaline to alkaline magmatism is indicative of a geodynamic switch from compressive to extensional regimes [75–78]. In the Victoria Land, the Larsen granodiorite, which extends south of the Fry glacier, has calc-alkaline affinities, similar to the ~505 Ma Bonney pluton (a portion of the GHI in

southern Victoria Land) comprising foliated diorite, monzodiorite, and granodiorite [49,79]. Although the Larsen granodiorite in the Central Victoria Land remains poorly studied, it probably has similar geochemical features. By contrast, the undeformed Irizar granite in the Central Victoria Land is dominated by potassic syenogranite with alkaline affinity and its genesis has been ascribed to remelting of a juvenile crust in a post-collisional setting [11,23]. Such a transition in magmatic composition and the different deformation features should be associated with the geodynamic change, from pre- to syn-collisional compression to post-collisional extension. Besides, granitoid-mafic dike associations are common in extensional tectonic regimes linked to post-collisional events [80–84]. The emplacement of the Irizar granite in the Central Victoria Land is accompanied by coeval and genetically related Vegetation lamprophyre dikes with alkaline affinity [11] (Figure 2). The Vegetation lamprophyre magma originated from the melting of previously enriched subcontinental lithospheric mantle, probably linked to asthenospheric upwelling during the post-collisional slab rollback and convective thinning and/or delamination of over-thickened lithosphere [11]. Thus, the Irizar granite is representative of post-collisional intrusive rocks in the Central Victoria Land [11], and the new geochronological data in this study confirm that the post-collisional extension had begun by ~508 Ma in the Central Victoria Land.

### 6.2. Implications for the Tectonic Evolution of the Ross–Delamerian Orogen

The Ross (and Delamerian) orogen is characterized by large volumes of Late Neoproterozoic to Early Paleozoic granitoid rocks, which have been widely accepted as important indicators of subduction and subsequent arc-continent collision along the eastern margin of Gondwana supercontinent [9,12,16,18,20,31,79]. Although the GHI rocks are collectively described as a suite of granitoids, in fact they vary marked in composition and emplacement ages [13,18,31]. Regional geochemical and isotopic variations in the GHI, as a result of increasing involvement of old continental crustal materials in the magma source from east to west, have indicated a continental-margin setting above the west-directed subduction zone [18,47,48]. Geochemistry of the igneous rocks and magmatic–stratigraphic relationships in the Delamerian orogen are also consistent with the westward subduction model [9,84,85], although some have suggested that the Delamerian orogen involved the development of an east-dipping subduction zone during Early Paleozoic [86,87]. Despite the increasing number of geochronological studies on the Ross granitoids during the last decade, the temporal–spatial distributions of magmatism along the Ross–Delamerian orogen and their tectonic implications remain poorly known.

To improve our understanding of the tectonic evolution of the Ross–Delamerian orogen, we compiled and synthesized as much U–Pb geochronological data as available from the literature [9,11,13,16,18–20,22,27,28,32,41,52–54,60,76,79,88–98] (Table S2), which are graphically shown in Figure 7. The geochronological data for the pre- to syn-tectonic calc-alkaline granitoids are systemically younger northward from ~590–520 Ma in the Central Transantarctic Mountains, through ~565–505 Ma in the Southern Victoria Land, and ~535–500 Ma in the Northern Victoria Land to ~520–490 Ma in the Southeast Australia (Figure 7). This is broadly consistent with the conclusions by Foden et al. [9] (2006) and Rocchi et al. [11,23] that the subduction propagated northward from ~540 Ma at the Ross orogen to ~514 Ma at its Southeast Australia counterpart. However, a much earlier initiation of the subduction-related magmatism in the Central Transantarctic Mountains than previously recognized is implied by the recent zircon U–Pb ages of ~590 Ma for the foliated muscovite-biotite granite clasts [18]. This is also in good agreement with previous speculation based on compositions and U–Pb ages for detrital zircons from the major Neoproterozoic and lower Paleozoic siliciclastic rocks in the Central Transantarctic Mountains [38].

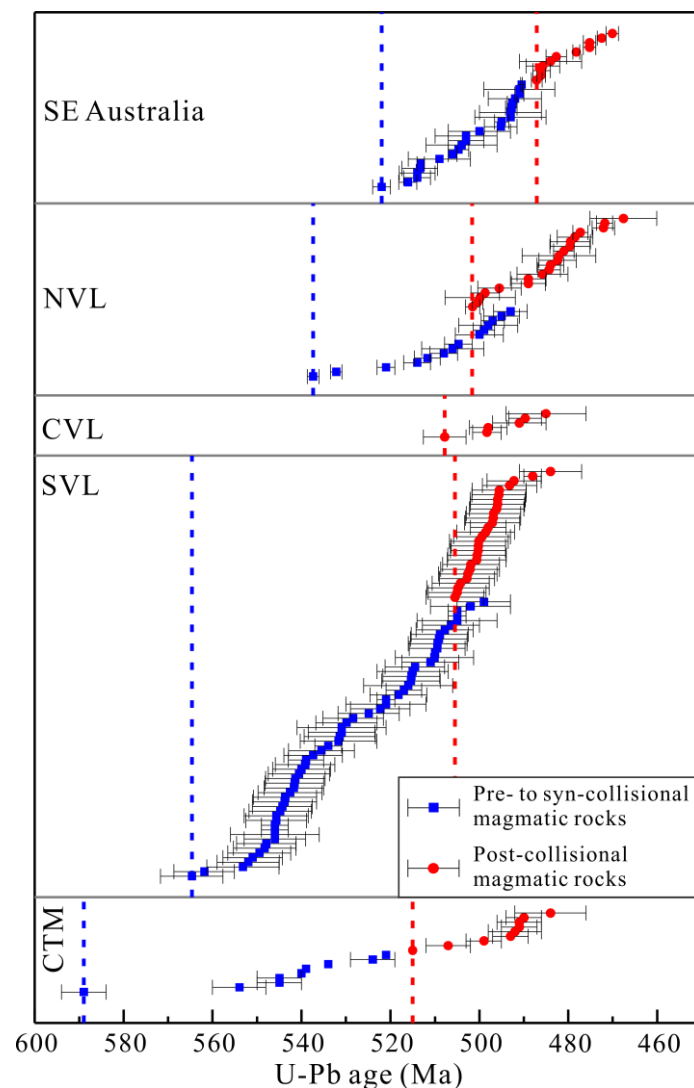


**Figure 7.** Summary of U-Pb isotopic age data for the Paleozoic granitoids in the Ross and Delamerian orogens. Sources of age data are listed in Table S2. Abbreviations: CTM, Central Transantarctic Mountains; CVL, Central Victoria Land; NVL, Northern Victoria Land; SE Australia, Southeastern Australia; SVL, Southern Victoria Land.

As mentioned previously, a synchronous transition to post-collisional extension at ~490–480 Ma in both the Ross (slab rollback) and Delamerian (slab tear) orogens was proposed by Foden et al. [9] and Rocchi et al. [11,23]. At the time, however, there were too few well-constrained ages for the post-collisional granitoids in Antarctica to establish the general time–space relations of the Ross magmatism. It also seems unlikely that the post-collisional extension occurred simultaneously along the >5000 km strike length of the Ross–Delamerian orogen. Numerical modeling and seismic tomography models have demonstrated that the slab break-off propagates laterally from one edge of the slab to the other [99,100], as is evidenced by the westward propagating slab tear in the Late Triassic Qinling Orogenic Belt, central China [101]. This model approximates the situation in the Ross–Delamerian Orogen. As is shown in Figure 7, the ages of the undeformed, post-collisional granitoids become systemically younger northward from ~515–484 Ma in the Central Transantarctic Mountains, through 508–468 Ma in the Victoria Land, to ~487–470 Ma in the Southeast Australia. This indicates the possible propagating northward transition from pre- and syn-collisional compression to post-collisional extension.

## 7. Conclusions

1. The undeformed Irizar syenogranite, representative of the post-collisional intrusive rocks in the Central Victoria Land, was emplaced between  $507.8 \pm 4.8$  Ma and  $489.7 \pm 3.7$  Ma.
2. The northward younger trend in emplacement ages of post-collisional granitoids in the Ross–Delamerian orogen is consistent with the northward transition and propagation, from pre- and syn-collisional compression to post-collisional extension.

**Supplementary Materials:** The following supporting information can be downloaded at: <https://www.mdpi.com/article/10.3390/min14030301/s1>, Table S1: Analytical results of SHRIMP zircon U-Pb dating for the Irizar syenogranite in the Central Victoria Land, Antarctica; Table S2: Summary of U-Pb isotopic age data for the Paleozoic granitoids in the Ross and Delamerian orogens.

**Author Contributions:** Conceptualization, S.C. and Y.C.; methodology, Y.C.; software, S.C. and H.Z.; validation, S.C. and S.Z.; formal analysis, S.L.; investigation, Y.C. and C.L.; resources, S.C. and Y.C.; data curation, S.C., Y.C. and W.W.; writing—original draft preparation, S.C.; writing—review and editing, Y.C. and S.L.; visualization, S.C.; supervision, Y.C.; project administration, Y.C.; funding acquisition, Y.C. All authors have read and agreed to the published version of the manuscript.

**Funding:** This research was funded by the National Key Research and Development Program of China, grant number 2022YFC2807405.

**Data Availability Statement:** Data are contained within the article and Supplementary Materials.

**Acknowledgments:** The Federal Institute for Geosciences and Natural Resources (Germany) is acknowledged for inviting us to participate in the 13th German Antarctic North Victoria Land Expedition (GANOVEX XIII 2018-19), and all the teammates are thanked for their help in sampling and field survey. We are grateful to Shouji Liu for his assistance in the SHRIMP zircon U-Pb dating.

**Conflicts of Interest:** The authors declare no conflicts of interest.

## References

1. Drexel, J.F.; Preiss, W.V. *The Geology of South Australia*; Bulletin; Geological Survey of South Australia: Adelaide, Australia, 1995; Volume 54, p. 347.
2. Turner, S.; Haines, P.; Foster, D.; Powell, R.; Sandiford, M.; Offler, R. Did the Delamerian Orogeny start in the Neoproterozoic? *J. Geol.* **2009**, *117*, 575–583. [[CrossRef](#)]
3. Cawood, P.A. Terra Australis Orogen: Rodinia breakup and development of the Pacific and Iapetus margins of Gondwana during the Neoproterozoic and Paleozoic. *Earth Sci. Rev.* **2005**, *69*, 249–279. [[CrossRef](#)]
4. Gibson, G.M.; Morse, M.P.; Ireland, T.R.; Nayak, G.K. Arc-continent collision and orogenesis in western Tasmanides: Insights from reactivated basement structures and formation of an ocean-continent transform boundary off western Tasmania. *Gondwana Res.* **2011**, *19*, 608–627. [[CrossRef](#)]
5. Palmeri, R.; Sandroni, S.; Godard, G.; Ricci, C.A. Boninite-derived amphibolites from the Lanterman-Mariner suture (northern Victoria Land, Antarctica): New geochemical and petrological data. *Lithos* **2012**, *140–141*, 200–223. [[CrossRef](#)]
6. Di Vincenzo, G.; Horton, F.; Palmeri, R. Protracted (~30 Ma) eclogite-facies metamorphism in northern Victoria Land (Antarctica): Implications for the geodynamics of the Ross/Delamerian Orogen. *Gondwana Res.* **2016**, *40*, 91–106. [[CrossRef](#)]
7. Stump, E.; White, A.J.R.; Borg, S.G. Reconstruction of Australia and Antarctica: Evidence from granites and recent mapping. *Earth Planet. Sci. Lett.* **1986**, *79*, 348–360. [[CrossRef](#)]
8. Boger, S.D.; Miller, J.M. Terminal suturing of Gondwana and the onset of the Ross–Delamerian Orogeny: The cause and effect of an Early Cambrian reconstruction of plate motions. *Earth Planet. Sci. Lett.* **2004**, *219*, 35–48. [[CrossRef](#)]
9. Foden, J.; Elburg, M.A.; Dougherty-Page, J.; Burt, A. The timing and duration of the Delamerian Orogeny: Correlation with the Ross Orogen and implications for Gondwana assembly. *J. Geol.* **2006**, *114*, 189–210. [[CrossRef](#)]
10. Glen, R.A.; Cooper, R.A. Evolution of the East Gondwana convergent margin in Antarctica, southern Australia and New Zealand from the Neoproterozoic to latest Devonian. *Earth Sci. Rev.* **2021**, *220*, 103687. [[CrossRef](#)]
11. Rocchi, S.; Di Vincenzo, G.; Ghezzi, C.; Nardini, I. Granite–lamprophyre connection in the latest stages of the Early Paleozoic Ross Orogeny (Victoria Land, Antarctica). *Geol. Soc. Am. Bull.* **2009**, *121*, 801–819. [[CrossRef](#)]
12. Goodge, J.W. Geological and tectonic evolution of the Transantarctic Mountains, from ancient craton to recent enigma. *Gondwana Res.* **2020**, *80*, 50–122. [[CrossRef](#)]
13. Gunn, B.M.; Warren, G. *Geology of Victoria Land between the Mawson and Mulock Glaciers, Antarctica*; New Zealand Geological Survey Bulletin: Wellington, New Zealand, 1962; Volume 71.

14. Allibone, A.H.; Wysoczanski, R. Initiation of magmatism during the Cambrian-Ordovician Ross orogeny in southern Victoria Land, Antarctica. *Geol. Soc. Am. Bull.* **2002**, *114*, 1007–1018. [[CrossRef](#)]
15. Goodge, J.W.; Walker, N.W.; Hansen, V.L. Neoproterozoic Cambrian basement-involved orogenesis within the Antarctic margin of Gondwana. *Geology* **1993**, *21*, 37–40. [[CrossRef](#)]
16. Encarnación, J.; Grunow, A. Changing magmatic and tectonic styles along the Paleo-Pacific margin of Gondwana and the onset of early Paleozoic magmatism in Antarctica. *Tectonics* **1996**, *15*, 1325–1341. [[CrossRef](#)]
17. Dallai, L.; Ghezzi, C.; Vesica, P.L. Oxygen isotope geochemistry of the Granite Harbour Intrusives, Wilson Terrane, Northern Victoria Land, Antarctica. *Mineral. Petrol.* **2002**, *75*, 223–241. [[CrossRef](#)]
18. Goodge, J.W.; Fanning, C.M.; Norman, M.; Bennett, V.C. Temporal, isotopic and spatial relations of early Paleozoic Gondwana-margin arc magmatism, central Transantarctic Mountains, Antarctica. *J. Petrol.* **2012**, *53*, 2027–2065. [[CrossRef](#)]
19. Cottle, J.M.; Cooper, A.F. The Fontaine Pluton: An early Ross Orogen calc-alkaline gabbro from southern Victoria Land, Antarctica. *N. Z. J. Geol. Geophys.* **2006**, *49*, 177–189. [[CrossRef](#)]
20. Foden, J.; Elburg, M.; Turner, S.; Clark, C.; Blades, M.L.; Cox, G.; Collins, A.S.; Wolff, K.; George, C. Cambro-Ordovician magmatism in the Delamerian orogeny: Implications for tectonic development of the southern Gondwana margin. *Gondwana Res.* **2020**, *81*, 490–521. [[CrossRef](#)]
21. Cawood, P.A.; Buchan, C. Linking accretionary orogenesis with supercontinent assembly. *Earth-Sci. Rev.* **2007**, *82*, 217–256. [[CrossRef](#)]
22. Giacomini, F.; Tiepolo, M.; Dallai, L.; Ghezzi, C. On the onset and evolution of the Ross-orogeny magmatism in North Victoria Land—Antarctica. *Chem. Geol.* **2007**, *240*, 103–128. [[CrossRef](#)]
23. Rocchi, S.; Bracciali, L.; Di Vincenzo, G.; Ghezzi, C. Arc accretion to the early Paleozoic Antarctic margin of Gondwana in Victoria Land. *Gondwana Res.* **2011**, *19*, 594–607. [[CrossRef](#)]
24. Di Vincenzo, G.; Rocchi, S. Origin and interaction of mafic and felsic magmas in an evolving late orogenic setting: The Early Paleozoic Terra Nova Intrusive Complex, Antarctica. *Contrib. Mineral. Petrol.* **1999**, *137*, 15–35. [[CrossRef](#)]
25. Grunow, A.; Encarnación, J. Cambro-Ordovician palaeomagnetic and geochronologic data from southern Victoria Land, Antarctica: Revision of the Gondwana apparent polar wander path. *Geophys. J. Int.* **2000**, *141*, 392–400. [[CrossRef](#)]
26. Di Vincenzo, G.; Viti, C.; Rocchi, S. The effect of chlorite interlayering on  $^{40}\text{Ar}$ - $^{39}\text{Ar}$  biotite dating: An  $^{40}\text{Ar}$ - $^{39}\text{Ar}$  laserprobe and TEM investigation of variably chloritised biotites. *Contrib. Mineral. Petrol.* **2003**, *145*, 643–658. [[CrossRef](#)]
27. Bomparola, R.M.; Ghezzi, C.; Belousova, E.; Griffin, W.L.; O'Reilly, S.Y. Resetting of the U-Pb zircon system in Cambro-Ordovician Intrusives of the Deep Freeze Range, Northern Victoria Land, Antarctica. *J. Petrol.* **2007**, *48*, 327–364. [[CrossRef](#)]
28. Chen, H.; Wang, W.; Zhao, Y. Constraints on early Paleozoic magmatic processes and tectonic setting of Inexpressible Island, Northern Victoria Land, Antarctica. *Adv. Polar Sci.* **2019**, *30*, 52–69.
29. Dalziel, I.W.D. Antarctica: A tale of two supercontinents: Annual Reviews of Earth and Planetary. *Sciences* **1992**, *20*, 501–526.
30. Flöttmann, T.; Gibson, G.M.; Kleinschmidt, G. Structural continuity of the Ross and Delamerian orogens of Antarctica and Australia along the margin of the paleo-Pacific. *Geology* **1993**, *21*, 319–322. [[CrossRef](#)]
31. Borg, S.G.; Stump, E.; Holloway, J.R. Granitoids of northern Victoria Land, Antarctica: A reconnaissance study of field relations, petrography and geochemistry. In *Geological Investigations in Northern Victoria Land, Antarctica*; Stump, E., Ed.; Antarctic Research Series; American Geophysical Union: Washington, DC, USA, 1986; Volume 46, pp. 115–188.
32. Foden, J.D.; Elburg, M.A.; Turner, S.P.; Sandiford, M.; O'Callaghan, J.; Mitchell, S. Granite production in the Delamerian Orogen, South Australia. *J. Geol. Soc.* **2002**, *159*, 557–575. [[CrossRef](#)]
33. Stump, E.; Laird, M.G.; Bradshaw, J.D.; Holloway, J.R.; Borg, S.G.; Lapham, K.E. Bowers graben and associated tectonic features cross northern Victoria Land, Antarctica. *Nature* **1983**, *304*, 334–336. [[CrossRef](#)]
34. Weaver, S.D.; Bradshaw, J.D.; Laird, M.G. Geochemistry of Cambrian volcanics of the Bowers Supergroup and implications for the Early Paleozoic tectonic evolution of northern Victoria Land, Antarctica. *Earth Planet. Sci. Lett.* **1984**, *68*, 128–140. [[CrossRef](#)]
35. Schüssler, U.; Bröcker, M.; Henjes-Kunst, F.; Will, T. P-T-t evolution of the Wilson Terrane metamorphic basement at Oates Coast, Antarctica. *Precambrian Res.* **1999**, *93*, 235–258. [[CrossRef](#)]
36. Ravich, M.G.; Klimov, L.V.; Soloviev, D.S. *The Precambrian of East Antarctica: Moscow (Trans. Scient. Research Institute of the Geology of the Arctic of the State Geological Committee), Russia*; Israel Program for Scientific Translations: Jerusalem, Israel, 1965; Volume 24.
37. Talarico, F.; Castelli, D. Relict granulites in the Ross Orogen of northern Victoria Land (Antarctica), I. Field occurrence, petrography and metamorphic evolution. *Precambrian Res.* **1995**, *75*, 141–156. [[CrossRef](#)]
38. Goodge, J.W.; Williams, I.S.; Myrow, P. Provenance of Neoproterozoic and lower Paleozoic siliciclastic rocks of the Central Ross Orogen, Antarctica: Detrital record of rift-, passive- and active-margin sedimentation. *Geol. Soc. Am. Bull.* **2004**, *116*, 1253–1279. [[CrossRef](#)]
39. Di Vincenzo, G.; Grande, A.; Rossetti, F. Paleozoic siliciclastic rocks from northern Victoria Land (Antarctica): Provenance, timing of deformation, and implications for the Antarctica-Australia connection. *Geol. Soc. Am. Bull.* **2014**, *126*, 1416–1438. [[CrossRef](#)]
40. Estrada, S.; Läufer, A.; Eckelmann, K.; Hofmann, M.; Gärtner, A.; Linnemann, U. Continuous Neoproterozoic to Ordovician sedimentation at the East Gondwana margin—Implications from detrital zircons of the Ross Orogen in northern Victoria Land, Antarctica. *Gondwana Res.* **2016**, *37*, 426–448. [[CrossRef](#)]

41. Paulsen, T.S.; Deering, C.; Sliwinski, J.; Bachmann, O.; Guillong, M. Detrital zircon ages from the Ross Supergroup, North Victoria Land, Antarctica: Implications for the tectonostratigraphic evolution of the Pacific-Gondwana margin. *Gondwana Res.* **2016**, *35*, 79–96. [[CrossRef](#)]
42. Buggisch, W.; Repetski, J.E. Uppermost Cambrian (?) and Tremadocian conodonts from Handler Ridge, Robertson Bay Terrane, North Victoria Land. *Antarct. Geol. Jahrb.* **1987**, *66*, 145–185.
43. Rossetti, F.; Storti, F.; Busetti, M.; Lisker, F.; Di Vincenzo, G.; Laeuffer, A.L.; Rocchi, S.; Salvini, F. Eocene initiation of Ross Sea dextral faulting and implications for East Antarctic neotectonics. *J. Geol. Soc.* **2006**, *163*, 119–126. [[CrossRef](#)]
44. Di Vincenzo, G.; Palmeri, R.; Talarico, F.; Andriessen, P.A.M.; Ricci, C.A. Petrology and geochronology of eclogites from the Lanterman Range, Antarctica. *J. Petrol.* **1997**, *38*, 1391–1417. [[CrossRef](#)]
45. Bracciali, L.; Di Vincenzo, G.; Rocchi, S.; Ghezzi, C. The Tiger Gabbro from northern Victoria Land, Antarctica: The roots of an island arc within the early Palaeozoic margin of Gondwana. *J. Geol. Soc.* **2009**, *166*, 711–724. [[CrossRef](#)]
46. Henjes-Kunst, F.; Tribuzio, R.; Gerdes, A. Early Cambrian oceanic island-arc magmatism at the paleo-Pacific margin of East Gondwana: Evidence from northern Victoria Land (Antarctica). *Lithos* **2021**, *382–383*, 105925. [[CrossRef](#)]
47. Borg, S.G.; Stump, E.; Chappell, B.W.; McCulloch, M.T.; Wyborn, D.; Armstrong, R.L.; Holloway, J.R. Granitoids of northern Victoria Land, Antarctica: Implications of chemical and isotopic variations to regional crustal structure and tectonics. *Am. J. Sci.* **1987**, *287*, 127–169. [[CrossRef](#)]
48. Borg, S.G.; DePaolo, D.J.; Smith, B.M. Isotopic structure and tectonics of the central Transantarctic Mountains. *J. Geophys. Res.* **1990**, *95*, 6647–6669. [[CrossRef](#)]
49. Cox, S.C.; Turnbull, I.M.; Isaac, M.J.; Townsend, D.B.; Smith Lyttle, B. *Geology of Southern Victoria Land Antarctica*; Institute of Geological and Nuclear Sciences 1:250,000 Geological Map 22. 1 Sheet + 135 p; GNS Science: Lower Hutt, New Zealand, 2012.
50. Black, L.P.; Sheraton, J.W. The influence of Precambrian source components on the U-Pb zircon age of a Palaeozoic granite from northern Victoria Land, Antarctica. *Precambrian Res.* **1990**, *46*, 275–293. [[CrossRef](#)]
51. Tonarini, S.; Rocchi, S. Geochronology of Cambro-Ordovician intrusives in northern Victoria Land: A review. *Terra Antart.* **1994**, *1*, 46–50.
52. Wang, W.; Hu, J.M.; Chen, H.; Yu, G.W.; Zhao, Y.; Liu, X.C. LA-ICP-MS zircon U-Pb ages and geological constraint of intrusive rocks from the Inexpressible Island, Northern Victoria Land, Antarctica. *Geol. Bull. China* **2014**, *33*, 2023–2031. (In Chinese with English Abstract).
53. Kim, D.; Yi, S.B.; Kim, H.; Kim, T.; Kim, T.; Lee, J.I. Geochemistry and geochronology of Early Paleozoic intrusive rocks in the Terra Nova Bay area, Northern Victoria Land, Antarctica. *Minerals* **2021**, *11*, 787. [[CrossRef](#)]
54. Gao, P.; Tang, L.M.; Chen, L. Geochemistry and zircon U-Pb ages of early Ordovician syenites from the Inexpressible Island, Antarctica and tectonic implications. *Front. Earth Sci.* **2023**, *10*, 966085. [[CrossRef](#)]
55. Vetter, U.; Roland, N.W.; Kreuzer, H.; Höhndorf, A.; Lenz, C.; Besang, H. Geochemistry, Petrography and Geochronology of the Cambro-Ordovician and Devonian-Carboniferous Granitoids of Northern Victoria Land, Antarctica. In *Antarctic Earth Science*; Oliver, R.L., James, P.R., Jago, J.B., Eds.; Australian Academy of Science: Canberra, Australia, 1983; pp. 140–143.
56. Stump, E. *The Ross Orogen of the Transantarctic Mountains*; Cambridge University Press: New York, NY, USA, 1995.
57. Capponi, G.; Montomoli, C.; Casale, S.; Simonetti, M. Geology of the northern Convoy Range, Victoria Land, Antarctica. *J. Maps* **2020**, *16*, 702–709. [[CrossRef](#)]
58. Skinner, D.N.B.; Ricker, J. The geology of the region between the Mawson and Priestley Glaciers, North Victoria Land, Antarctica. *N. Z. J. Geol. Geophys.* **1968**, *11*, 1009–1040. [[CrossRef](#)]
59. Renna, M.R.; Tiepolo, M.; Tribuzio, R. In situ U-Pb geochronology of baddeleyite-zircon pairs using laser-ablation ICPMS: The case-study of quartz gabbro from Varney Nunatak (central Victoria Land, Antarctica). *Eur. J. Mineral.* **2011**, *23*, 223–240. [[CrossRef](#)]
60. Rocchi, S.; Di Vincenzo, G.; Ghezzi, C. The Terra Nova Intrusive Complex (Victoria Land, Antarctica), with 1:50,000 Geopetrographic Map. *Terra Antart. Rep.* **2004**, *10*, 51.
61. Middlemost, E.A.K. Naming materials in the magma/igneous rock system. *Earth Sci. Rev.* **1994**, *37*, 215–224. [[CrossRef](#)]
62. Streckeisen, A. To each plutonic rock its proper name. *Earth Sci. Rev.* **1976**, *12*, 1–33. [[CrossRef](#)]
63. Williams, I.S. U-Th-Pb geochronology by ion microprobe. In *Applications of Microanalytical Techniques to Understanding Mineralizing Processes*; McKibben, M.A., Shanks, W.C., Ridley, W.I., Eds.; Review of Economic Geology; Economic Geology Pub Co.: Lancaster, PA, USA, 1998; Volume 7, pp. 1–35.
64. Ballard, J.R.; Palin, J.M.; Williams, I.S.; Campbell, I.H.; Faunes, A. Two ages of porphyry intrusion resolved for the super-giant Chuquibambilla copper deposit of northern Chile by ELA-ICP-MS and SHRIMP. *Geology* **2001**, *29*, 383–386. [[CrossRef](#)]
65. Nasdala, L.; Hofmeister, W.; Norberg, N.; Martinson, J.M.; Corfu, F.; Dörr, W.; Kamo, S.L.; Kennedy, A.K.; Kronz, A.; Reiners, P.W. Zircon M257—A Homogeneous Natural Reference Material for the Ion Microprobe U-Pb Analysis of Zircon. *Geostand. Geoanal. Res.* **2008**, *32*, 247–265. [[CrossRef](#)]
66. Black, L.P.; Kamo, S.L.; Allen, C.M.; Aleinikoff, J.N.; Davis, D.W.; Korsch, R.J.; Foudoulis, C. TEMORA 1: A new zircon standard for Phanerozoic U-Pb geochronology. *Chem. Geol.* **2003**, *200*, 155–170. [[CrossRef](#)]
67. Ludwig, K.R. *Squid 1.02: A User's Manual*; Berkeley Geochronology Centre Special Publication: Berkeley, CA, USA, 2001; pp. 1–19.
68. Hoskin, P.W.O.; Schaltegger, U. The composition of zircon and igneous and metamorphic petrogenesis. *Rev. Mineral. Geochem.* **2003**, *53*, 27–62. [[CrossRef](#)]
69. Hanchar, J.M.; Miller, C.F. Zircon zonation patterns as revealed by cathodoluminescence and backscattered electron images: Implications for interpretation of complex histories. *Chem. Geol.* **1993**, *110*, 1–13. [[CrossRef](#)]

70. White, L.T.; Ireland, T.R. High-uranium matrix effect in zircon and its implications for SHRIMP U-Pb age determinations. *Chem. Geol.* **2012**, *306–307*, 78–91. [[CrossRef](#)]
71. Miller, W.M.; Fallick, A.E.; Leake, B.E.; Macintyre, R.M.; Jenkin, G.R.T. Fluid disturbed hornblende K-Ar ages from the Dalradian rocks of Connemara, Western Ireland. *J. Geol. Soc.* **1991**, *148*, 985–992. [[CrossRef](#)]
72. Jenkin, G.R.T.; Ellam, R.M.; Rogers, G.; Stuart, F.M. An investigation of closure temperature of the biotite Rb-Sr system: The importance of cation exchange. *Geochim. Cosmochim. Acta* **2001**, *65*, 1141–1160. [[CrossRef](#)]
73. Chen, W.; Wan, Y.S.; Li, H.Q.; Zhang, Z.Q.; Dai, T.M.; Shi, Z.E.; Sun, J.B. Isotope geochronology: Technique and application. *Acta Geol. Sin.* **2011**, *85*, 1917–1947, (In Chinese with English Abstract).
74. Harris, N.B.W.; Pearce, J.A.; Tindle, A.G. Geochemical characteristics of collision zone magmatism. In *Collision Tectonics*; Coward, M.P., Ries, A.C., Eds.; Geological Society of London, Special Publications: London, UK, 1986; Volume 19, pp. 67–82.
75. Avigad, D.; Gvirtzman, Z. Late Neoproterozoic rise and fall of the northern Arabian–Nubian shield: The role of lithospheric mantle delamination and sub-sequent thermal subsidence. *Tectonophysics* **2009**, *477*, 217–228. [[CrossRef](#)]
76. Hagen-Peter, G.; Cottle, J.M. Synchronous alkaline and subalkaline magmatism during the late Neoproterozoic-early Paleozoic Ross orogeny, Antarctica: Insights into magmatic sources and processes within a continental arc. *Lithos* **2016**, *262*, 677–698. [[CrossRef](#)]
77. Zoheir, B.A.; Lehmann, B.; Emam, A.; Radwan, A.; Zhang, R.; Bain, W.M.; Steele-MacInnis, M.; Nolte, N. Extreme fractionation and transitional magmatic-hydrothermal processes in the Abu Dabbab rare-metal granite system, Eastern Desert, Egypt. *Lithos* **2020**, *352–353*, 105329. [[CrossRef](#)]
78. Lehmann, B.; Zoheir, B.A.; Neymark, L.A.; Zeh, A.; Emam, A.; Radwan, A.M.; Zhang, R.; Moscati, R.J. Monazite and cassiterite U-Pb dating of the Abu Dabbab raremetal granite, Egypt: Late Cryogenian metalliferous granite magmatism in the Arabian-Nubian Shield. *Gondwana Res.* **2020**, *84*, 71–80. [[CrossRef](#)]
79. Allibone, A.H.; Cox, S.C.; Smille, R.T. Granitoids of the Dry Valleys area, southern Victoria Land: Geochemistry and evolution along the early Paleozoic Antarctic Craton margin. *N. Z. J. Geol. Geophys.* **1993**, *36*, 299–316. [[CrossRef](#)]
80. Eby, G.N. Chemical subdivision of the A-type granitoids: Petrogenetic and tectonic implications. *Geology* **1992**, *20*, 641–644. [[CrossRef](#)]
81. Yang, J.H.; Sun, J.F.; Chen, F.K.; Wilde, S.A.; Wu, F.Y. Sources and petrogenesis of late Triassic dolerite dikes in the Liaodong Peninsula: Implications for post-collisional lithosphere thinning of the Eastern North China Craton. *J. Petrol.* **2007**, *48*, 1973–1997. [[CrossRef](#)]
82. Tang, G.J.; Chung, S.L.; Wang, Q.; Wyman, D.A.; Dan, W.; Chen, H.Y.; Zhao, Z.H. Petrogenesis of a Late Carboniferous mafic dike–granitoid association in the western Tianshan: Response to the geodynamics of oceanic subduction. *Lithos* **2014**, *202–203*, 85–99. [[CrossRef](#)]
83. Sun, Y.G.; Li, B.L.; Sun, F.Y.; Ding, Q.F.; Qian, Y.; Li, L.; Xu, Q.L.; Li, Y.J. Geochronology, geochemistry, and Hf isotopic compositions of early Permian syenogranite and diabase from the northern Great Xing’an Range, northeastern China: Petrogenesis and tectonic implications. *Can. J. Earth Sci.* **2020**, *57*, 1478–1491. [[CrossRef](#)]
84. Kemp, A.I.S. Plutonic boninite-like rocks in an anatectic setting: Tectonic implications for the Delamerian orogen in southeastern Australia. *Geology* **2003**, *31*, 371–374. [[CrossRef](#)]
85. Squire, R.J.; Wilson, C.J.L.; Dugdale, L.J.; Jupp, B.J.; Kaufman, A.L. Cambrian backarc-basin basalt in western Victoria related to evolution of a continent-dipping subduction zone. *Aust. J. Earth Sci.* **2006**, *53*, 707–719. [[CrossRef](#)]
86. Crawford, A.J.; Berry, R.F. Tectonic implications of late Proterozoic–early Paleozoic igneous rock associations in western Tasmania. *Tectonophysics* **1992**, *214*, 37–56. [[CrossRef](#)]
87. Vandenberg, A.H.M.; Willman, C.E.; Maher, S.; Simons, B.A.; Cayley, R.A.; Taylor, D.H.; Morand, V.J.; Moore, D.H.; Radojkovic, A. *The Tasman Fold Belt System in Victoria*; Geological Survey of Victoria Special Publication: Melbourne, Australia, 2000; p. 462.
88. Cottle, J.M.; Cooper, A.F. Geology, geochemistry, and geochronology of an A-type granite in the Mulock Glacier area, southern Victoria Land, Antarctica. *N. Z. J. Geol. Geophys.* **2006**, *49*, 191–202. [[CrossRef](#)]
89. Cox, S.C.; Parkinson, D.L.; Allibone, A.H.; Cooper, A.F. Isotopic character of Cambro-Ordovician plutonism, southern Victoria Land, Antarctica. *N. Z. J. Geol. Geophys.* **2000**, *43*, 501–520. [[CrossRef](#)]
90. Fanning, C.M. *Single Grain Dating of a Granite Sample from Cape Willoughby, Kangaroo Island*; Prise Laboratories, Australian National University Progress Report 89-060; South Australia Department of Mines and Energy, Open File Envelope: Canberra, Australia, 1990; Volume 8828, pp. 29–32.
91. Fioretti, A.M.; Capponi, G.; Black, L.P.; Varne, R.; Visona, D. Surgeon island granite SHRIMP zircon ages: A clue for the Cambrian tectonic setting and evolution of the Paleopacific margin of Gondwana (northern Victoria Land, Antarctica). *Terra Nova* **2005**, *17*, 242–249. [[CrossRef](#)]
92. Foden, J.; Sandiford, M.; Dougherty-Page, J.; Williams, I. Geochemistry and geochronology of the Rathjen Gneiss: Implications for the early tectonic evolution of the Delamerian Orogen. *Aust. J. Earth Sci.* **1999**, *46*, 377–389. [[CrossRef](#)]
93. Gao, P.; Tang, L.M.; Chen, L.; Yuan, T.; Fang, Y.X. Geochronology and geochemistry of the dioritic rocks from the Inexpressible Island, Northern Victoria Land, Antarctica and their geological implications. *Acta Petrol. Sin.* **2022**, *38*, 923–941, (in Chinese with English abstract).
94. Hall, C.E.; Cooper, A.F.; Parkinson, D.L. Early Cambrian carbonatite in Antarctica. *J. Geol. Soc.* **1995**, *152*, 721–728. [[CrossRef](#)]

95. Ireland, T.; Morand, V.; Gibson, G. Results from some recent SHRIMP U-Pb zircon dating of rocks from the Glenelg Zone of western Victoria. *Geol. Surv. Vic. Tech. Rec.* **2002**, *2*, 1–23.
96. Jenkins, R.; Cooper, J.A.; Compston, W. Age and biostratigraphy of Early Cambrian tuffs from SE Australia and southern China. *J. Geol. Soc.* **2002**, *159*, 645–658. [[CrossRef](#)]
97. Read, S.E.; Cooper, A.F.; Walker, N.W. *Geochemistry and U-Pb Geochronology of the Neoproterozoic-Cambrian Koettlitz Glacier Alkaline Province, Royal Society Range, Transantarctic Mountains, Antarctica*; Royal Society of New Zealand Bulletin: Wellington, New Zealand, 2002; Volume 35, pp. 143–151.
98. Stump, E.; Gootee, B.; Talarico, F. Tectonic model for development of the Byrd Glacier discontinuity and Surrounding regions of the Transantarctic Mountains during the Neoproterozoic—Early Paleozoic. In *Antarctica: Contributions to Global Earth Sciences*; Fütterer, D.K., Damaske, D., Kleinschmidt, G., Miller, H., Tessensohn, F., Eds.; Springer: Berlin/Heidelberg, Germany, 2006; pp. 45–54.
99. Wortel, M.J.R.; Spakman, W. Subduction and slab detachment in the Mediterranean–Carpathian region. *Science* **2000**, *290*, 1910–1917. [[CrossRef](#)]
100. Van Hunen, J.; Allen, M.B. Continental collision and slab break-off: A comparison of 3-D numerical models with observations. *Earth Planet. Sci. Lett.* **2011**, *302*, 27–37. [[CrossRef](#)]
101. Hu, F.Y.; Liu, S.W.; Zhang, W.Y.; Deng, Z.B.; Chen, X. A westward propagating slab tear model for Late Triassic Qinling Orogenic Belt geodynamic evolution: Insights from the petrogenesis of the Caoping and Shahewan intrusions, central China. *Lithos* **2016**, *262*, 486–506. [[CrossRef](#)]

**Disclaimer/Publisher’s Note:** The statements, opinions and data contained in all publications are solely those of the individual author(s) and contributor(s) and not of MDPI and/or the editor(s). MDPI and/or the editor(s) disclaim responsibility for any injury to people or property resulting from any ideas, methods, instructions or products referred to in the content.